PALEONTOLOGY

Biogenic origin of secondary eggshell units in dinosaur eggshells elucidates lost biomineralization process in maniraptoran dinosaurs

Shukang Zhang[1,2]*, Seung Choi[1,2]†, Noe-Heon Kim[3]‡, Junfang Xie[4], Yong Park[5], Oliver Plümper[6], Albert G. Sellés[7]

Secondary eggshell units, though rarely observed in modern avian eggshells, are marked structures in non-avian dinosaur eggshells that offer valuable paleobiological insights. Despite their significance, the origins of secondary eggshell units remain understudied, leading to debates in paleontology, including the hypothesis of an abiogenic origin for these structures. Here, we demonstrate that secondary eggshell units in non-avian dinosaur eggshells are biogenic in nature, based on analyses using advanced microscopic techniques. The structural characteristics of these units suggest a formation mechanism similar to that of turtle and crocodile eggshells, with matrix fibers likely initiating their development. Furthermore, a diminishing presence of secondary eggshell units in non-avian maniraptoran dinosaurs points to the evolution of a more refined physiological process for eggshell formation in this lineage. These findings shed light on the evolutionary trajectory of eggshell biomineralization in dinosaurs and their close relatives.

INTRODUCTION

Biominerals are invaluable for natural history because they are easily fossilized and preserved, so a substantial amount of (paleo)biological information preserved in biomineral can be used to reconstruct the biology of extinct organisms (*1*, *2*). For amniotic vertebrates, eggshells, bones, and teeth are one of the three representative biominerals. Fossil eggshells not only provide morphological data (*3*–*5*) but also paleobiological knowledge, such as paleoproteomics for the identification of controversial eggshells (*6*) and paleophysiology regarding the body temperature of egg-laying dinosaurs (*7*–*9*). Notably, physiological processes are strongly involved in biomineralization (*10*), and thus, fossil eggshells provide rare chances to infer the physiological processes of extinct organisms (*5*, *11*–*14*).

All archelosaur eggshells share a common formation process: Eggshell units [specifically, primary eggshell units (PEUs)] (Fig. 1A) composed of radial calcium carbonate nucleate on organic cores in shell membranes and grow outward with microstructural transformation. These are the main type of eggshell units present in all archelosaurs, including maniraptoran dinosaurs (*3*). In rare cases, secondary eggshell units (SEUs) (Fig. 1, B to D) that nucleate at areas other than the shell membrane [e.g., superimposed eggshell units (*11*) and extra-spherulite (*15*, *16*)] have been observed in modern chelonian, crocodilian, and (very rarely) avian eggshells (*15*, *17*–*19*). In the fossil record, eggshells of some non-avian dinosaurs, hereafter simply dinosaurs, also contain SEUs; however, their evolutionary relationship has rarely been studied.

The origin of SEUs has not been resolved. SEUs have been widely documented in East Asian oofamilies with porous eggshell microstructures and were regarded as biogenic structures and as intrinsic characteristics of several oofamilies (*5*, *11*, *20*–*26*). Some of these oofamilies including Dendroolithidae, Dictyoolithidae, Faveoloolithidae, and Youngoolithidae have been interpreted to have a unique eggshell formation mechanism: The eggshell units and fibers of shell membrane form simultaneously, rather than sequentially, and new nucleation centers repeatedly form among the organic fibers, resulting in superimposed SEUs (Fig. 1, E to J) (*5*, *11*, *20*). In stalicoolithid eggshells, new nucleation centers are only formed in the pore canals and near the outer surface of the eggshell because of the tightly arranged PEUs (*23*).

By contrast, an abiogenic origin for SEUs was suggested based mainly on the SEUs in megaloolithid eggshells laid by titanosaurs (Sauropoda, Dinosauria) (*27*, *28*). Grellet-Tinner *et al.* (*29*) studied the SEUs of *Megaloolithus* from Spain and Argentina using a combination of polarized light microscopy (PLM), scanning electron microscopy (SEM), and cathodoluminescence (CL). They hypothesized that SEUs are byproducts of diagenesis and that organic matter triggered the formation of the pseudo-cores of SEUs. Moreno-Azanza *et al.* (*16*) studied SEUs in Spanish *Megaloolithus* by additionally using electron backscatter diffraction (EBSD), which provided insightful results. Namely, despite PEUs and SEUs not being unequivocally distinguished in CL images (*16*, *29*), Moreno-Azanza *et al.* (*16*) provided a hypothesis for the abiogenic origin of SEUs based on the following observations: (i) SEUs lack organic cores and have less inclusions of organic matter than those of PEUs; (ii) compared with (truly biogenic) PEUs, SEUs have fewer low-angle grain boundaries; (iii) most SEUs are restricted to locations more exposed to dissolution; and (iv) most SEUs grow at an angle to the general growth direction of PEUs without disturbing the growth of adjacent PEUs. Recently, in a study of faveoloolithid eggshells, Kim *et al.* (*26*)

[1]Key Laboratory of Vertebrate Evolution and Human Origins of Chinese Academy of Sciences, Institute of Vertebrate Paleontology and Paleoanthropology, Chinese Academy of Sciences, Beijing 100044, China. [2]CAS Center for Excellence in Life and Paleoenvironment, Beijing 100044, China. [3]School of Earth and Environmental Sciences, Seoul National University, Seoul 08826, South Korea. [4]Zhejiang Museum of Natural History, Hangzhou, Zhejiang 310012, China. [5]Research Institute of Basic Sciences, Seoul National University, Seoul 08826, South Korea. [6]Department of Earth Sciences, Utrecht University, Utrecht 3584 CB, Netherlands. [7]Institut Català de Paleontologia Miguel Crusafont, Universtat Autònoma de Barcelona, Cerdanyola de Vallès 08193, Spain.
*Corresponding author. Email: zhangshukang@ivpp.ac.cn
†Present address: Research Institute of Basic Sciences, Seoul National University, Seoul 08826, South Korea.
‡Present address: Department of Geosciences, Princeton University, Princeton, NJ 08544, USA.

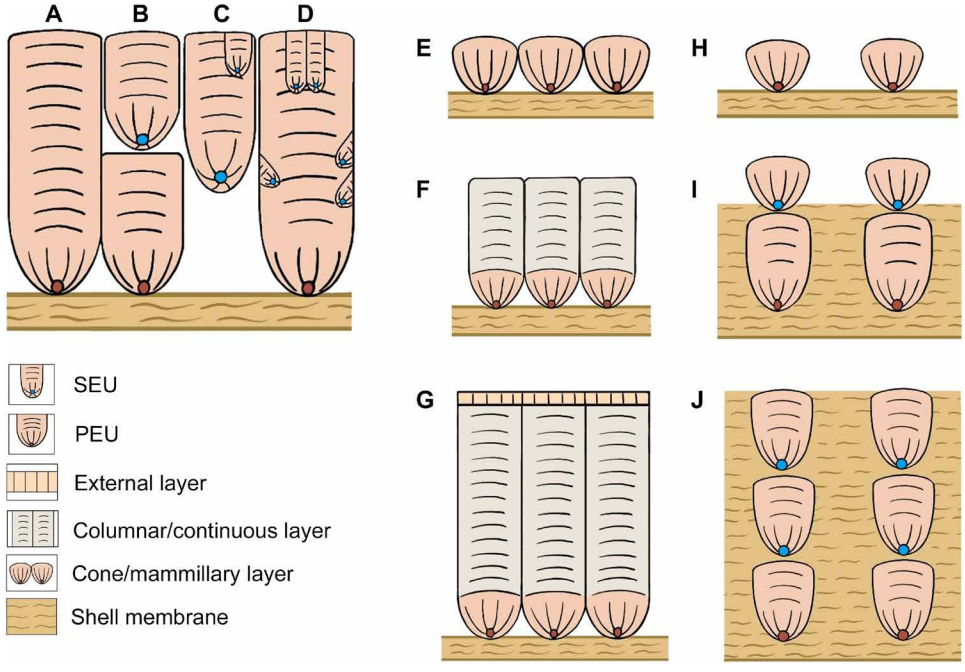

Fig. 1. Schematic drawing showing the basic information about the eggshell microstructure. (**A** to **D**) PEU and types of SEUs. (**E** to **J**) Comparison of the proposed formation process of avian eggshells and dinosaur eggshells containing SEUs. (A) PEU. (B) SEU superimposed on PEU. (C) SEU growing in pore canal and a smaller SEU embedded in it. (D) Small SEUs (extra-spherulites) embedded in PEU. (E to G) The formation process of avian eggshells: Shell membrane, cone, columnar, and external layers formed sequentially in avian eggshells. (H to J) Formation process of dinosaur eggshells containing SEUs that was proposed in previous works (*11*, *20*): Shell membrane and corresponding layers of eggshell units may have formed simultaneously in dinosaur eggshells containing SEUs.

described SEUs with similar characteristics to those of megaloolithid eggshells, such as dominant high-angle grain boundaries (*16*). Thereby, Kim *et al.* (*26*) also proposed an abiogenic origin interpretation for SEUs.

However, the frequent presence of SEUs in eggshells under spatiotemporally diverse taphonomic settings (*5*, *15*, *16*, *25*, *26*, *29*–*32*), the limited available in-depth research on SEUs, and the still developing methodologies for testing the biogenicity of calcium carbonate in fossil eggshells result in skepticism of the abiogenic interpretation of SEUs. If SEUs were derived from the biomineralization process of dinosaurs, this supports that the formation of some dinosaur eggshells was meaningfully different from that of maniraptoran dinosaur (including birds) eggshells (*5*, *11*, *20*), which are characterized by the near absence of SEUs (*33*). Furthermore, considering that eggshell biomineralization is the outcome of the physiological evolution of egg layers, a biogenic interpretation for the origin of SEUs indirectly provides a chance to explore the disparate biomineralization strategies and reproductive evolutionary experimentation along reptilian eggshell evolution.

Here, we investigated the microstructure, ultrastructure, and crystallographic features of SEUs in diverse dinosaur eggshells from China and Spain using a combination of PLM, SEM, transmission electron microscopy (TEM), CL, and EBSD, and compared the micro- and ultrastructures of dinosaur eggshells with those of turtle and crocodile eggshells (i) to test the biogenicity of SEUs and further discuss their functions, (ii) to hypothesize about the formation process of dinosaur eggshells and their SEUs, and (iii) to discuss the evolution of SEUs.

RESULTS

Several different Chinese dinosaur eggshells containing SEUs were used here, including *Dictyoolithus hongpoensis* (IVPP RV94001), *Faveoloolithus ningxiaensis* (IVPP V4709), *Multifissoolithus megadermus* (IVPP V2337), *Ovaloolithus mixtistriatus* (IVPP V736), *Parafaveoloolithus microporus* (IVPP V16857), *Paraspheroolithus irenensis* (IVPP V731), *Stromatoolithus pinglingensis* (IVPP V33471), and *Youngoolithus xiaguanensis* (IVPP V5783), which are housed at the Institute of Vertebrate Paleontology and Paleoanthropology (IVPP; Beijing, China); dictyoolithid (ZMNH M8889) and stalicoolithid (ZMNH M8102 and M8929) eggshells, which are housed at the Zhejiang Museum of Natural History (ZMNH; Zhejiang, China); *Stalicoolithus shifengensis* (TTM 29), which is housed at the Tiantai Museum (TTM; Zhejiang, China); and *Placoolithus tumiaolingensis* (TML 4) collected from Tumiaoling (TML; Hubei, China). In addition, to conduct a comparative study, *Megaloolithus siruguei* (IVPP V31358) from Pinyes, Coll de Nargo, Spain was collected and analyzed (see Supplementary Text for the selection criteria; see table S1 for the localities and horizons of all the fossil eggshells).

Several turtle, crocodile, and avian eggshells were prepared for comparison. Specimens include a Late Cretaceous fossil turtle egg, *Testudoolithus zelenitskyae* (MOR 710), housed at the Museum of the Rockies (MOR; Montana, USA), and eggshells of modern turtles (*Astrochelys radiata*, *Chelydra serpentine*, and *Chelonia mydas* from personal collections), modern crocodile (*Caiman crocodilus*) that is part of the egg collection of the Evolution and Optics of Nanostructures laboratory at Ghent University, and modern birds (*Struthio camelus*, IVPP E27; *Dromaius novaehollandiae*, IVPP E25) housed at IVPP.

The primary data used in this study include EBSD maps. Figure 2 presents the basic information about the EBSD maps used in this study.

Comparison of biogenic and abiogenic parts of dinosaur eggshells using a combination of microscopic techniques

PLM and EBSD

The combined use of PLM images, EBSD band contrast (BC), and kernel average misorientation (KAM) maps provides an effective way to test the biogenicity of SEUs (Fig. 3). Here, we define "biogenic calcite" as made by biomineralization process of amniotes. All other mineralization observed in this study (i.e., physicochemical process without biotically influenced precipitation) is referred to as "abiogenic calcite."

In PLM images, biogenic calcite is colored due to degraded organic matter (*34*, *35*), while abiogenic calcite is translucent (Fig. 3, A and E). In the inverse pole figure (IPF) Y images, the abiogenic calcite that fills the pore canals is usually polygonal in shape and has various *c*-axis directions. In contrast, the biogenic calcite has a consistent *c*-axis direction that is oriented parallel to the main growth direction of the eggshell (Fig. 3, B and F) (*16*). On combined band contrast and grain boundary (BC + GB) maps, the abiogenic calcite grain is characterized by a plain gray color, while the biogenic parts have textured gray scales that sometimes accompany small-angle (5° to 10°) grain boundaries (Fig. 3, C and G). These different features on the BC + GB map are consistently present on KAM maps. In the abiogenic parts, there are few high KAM lines, and even if high KAM lines are present, the lines do not have a dominant orientation. By contrast, the biogenic parts contain abundant high KAM lines, the directions of which are very similar to the *c*-axis direction of the biogenic calcite (Fig. 3, D and H).

SEM and TEM

The SEUs and abiogenic calcite have different degrees of texture and porosity on both the microscale and nanoscale levels. In the backscattered electron image of the focused ion beam (FIB) foil taken using a FIB-SEM, clear growth lines are visible in the SEUs of the *Placoolithus* eggshell (Fig. 3, I and J). In contrast, the abiogenic calcite surrounding the SEUs lacks growth lines. In the highly magnified TEM image, the SEUs are more porous than the surrounding abiogenic calcite (Fig. 3K).

CL

CL analysis has been conventionally used to detect abiogenic calcite in fossil eggshells (*7*, *16*, *26*, *29*, *36*), but it is worth mentioning that CL does not always distinguish between biogenic and abiogenic calcite (*2*, *37*). Most of the abiogenic calcite filling the pore canals/cavities of the *Faveoloolithus*, *Placoolithus,* and stalicoolithid eggshells do not exhibit orange luminescence (fig. S1, A to C), probably due to a lack of Mn^{2+} (CL reaction activator) or a large amount of Fe^{2+} (CL reaction quencher) (*37*). By contrast, the abiogenic calcite filling the cavities/pore canals of the dictyoolithid and *Youngoolithus* eggshells exhibit bright orange luminescence (fig. S1, D to F). The small vertical cracks with bright orange luminescence are extensively distributed in the eggshell units of *Youngoolithus*, indicating the influence of Mn-rich fluid (fig. S1F). Some of the growth lines of the *Placoolithus* and stalicoolithid eggshells exhibit bright orange luminescence, while others exhibit faint luminescence (Fig. 3, L to N, and fig. S1). The SEUs and PEUs exhibit faint orange luminescence for all the analyzed specimens. The luminescence levels of the SEUs and adjacent biogenic PEUs are not obviously different (Fig. 3, L to N, and fig. S1), which is similar to the results of Moreno-Azanza *et al.* (*16*).

SEUs of dinosaur eggshells

Here, we document the SEUs of dinosaur eggshells to provide information for discussing their biogenic or abiogenic origins and growth patterns of the SEUs. We describe the eggshells based on their porosity level, especially because the growth patterns of the SEUs are different.

Highly porous eggshells

The highly porous eggshells analyzed in this study are from six ootaxa: Dictyoolithidae, *Faveoloolithus*, *Multifissoolithus*, *Parafaveoloolithus*, *Placoolithus,* and *Youngoolithus*, whose pore canals or cavities between eggshell units are numerous and large (see figs. S2 to S6 for additional images). The SEUs are cone-shaped and originate within

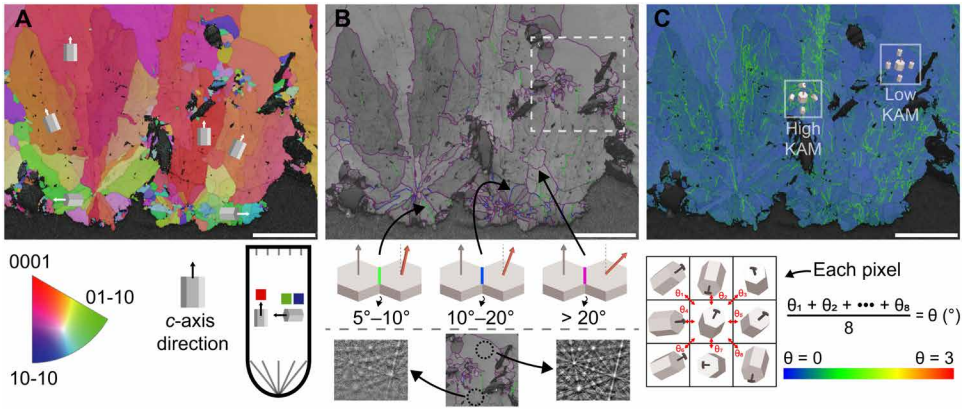

Fig. 2. Basic information about EBSD images. (**A**) Inverse pole figure (IPF) Y map of calcite. The colors of the calcite grain represent the *c*-axis direction, and the black regions indicate an absence of calcite. Red means that the *c* axis is perpendicular to the eggshell surface, while green and blue mean that the *c* axis is parallel to the eggshell surface. (**B**) Grain boundary (GB) map overlying band contrast (BC) map (grayscale). The colored lines mark the calcite grain boundaries. Green lines represent low-angle grain boundaries, while purple lines represent high-angle grain boundaries. On the BC map, the bright region in a single calcite grain is equivalent to clear Kikuchi band signals. In contrast, the dark (or textured) region has comparatively poorer Kikuchi band signals. (**C**) Kernel average misorientation (KAM) map showing the distribution of KAM values. When a pixel is surrounded by neighboring pixels with divergent crystallographic orientations, the central pixel has a high KAM value. Scale bars, 100 μm.

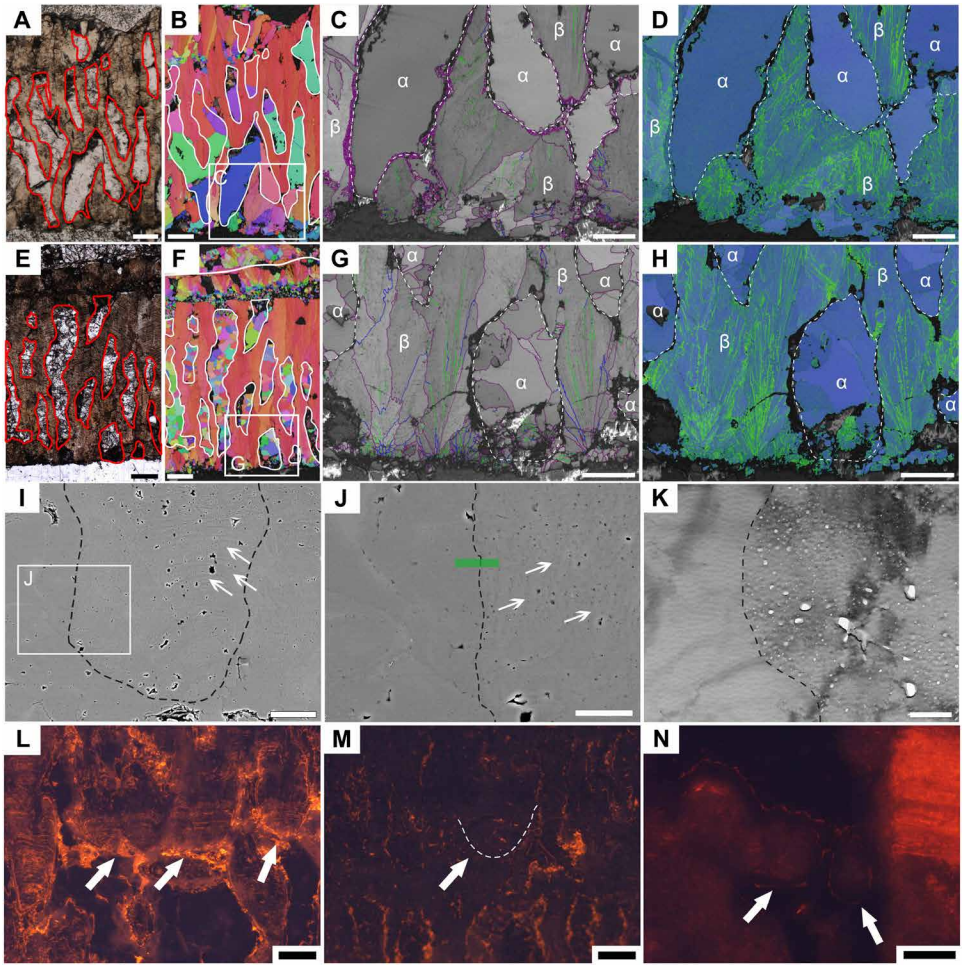

Fig. 3. PLM, EBSD, SEM, TEM, and CL analyses of biogenic and abiogenic parts of eggshell. (**A** to **H**) PLM and EBSD analyses of dictyoolithid (ZMNH M8889) (A to D) and *Youngoolithus* (IVPP V5783) (E to H) eggshells. (A and E) Radial thin sections under normal light. The biogenic calcite is colored, while the abiogenic calcite is translucent, and the red lines indicate the boundaries between them. (B and F) IPF Y maps. Note that the abiogenic calcite (marked with white lines) usually exhibits various orientations. (C and G) BC + GB and (D and H) KAM maps of PEUs. Note that the abiogenic calcite (marked with α) has plain gray colors on the BC + GB map and low KAM values, while the biogenic calcite (β) has textured gray scales with small-angle (5° to 10°) grain boundaries on the BC + GB map and high KAM values. (**I**) Backscattered electron image of an SEU in a *Placoolithus* eggshell (TML 4), showing clear growth lines in the biogenic part (arrows). (**J**) Enlargement of the edge area of the SEU. Note that the SEU is more porous (right part). The arrows indicate the growth lines. The green rectangle indicates the target area of the TEM analysis. (**K**) TEM image of the SEU, showing the porous (white spots) calcite in the SEU (right) and the nonporous abiogenic calcite (left). The dashed lines indicate the boundary between the SEU and abiogenic calcite. CL images of (**L**) *Placoolithus* (TML 4), (**M**) *Faveoloolithus* (IVPP V 4709), and (**N**) stalicoolithid (ZMNH M8102) eggshells. The arrows indicate the SEUs. The dashed line in (M) indicates the contour of the SEU. Scale bars, 200 μm [(A), (B), (E), and (F)], 100 μm [(C), (D), (G), (H), and (N)], 50 μm (I), 15 μm (J), 500 nm (K), and 150 μm [(L) and (M)].

the cavities between the PEUs or other SEUs (Fig. 4, A and B), or are superimposed on the PEUs and other SEUs (Fig. 4, C and D). Some of the SEUs are grouped in the middle and outer portions of the eggshells (Fig. 4A). In contrast, others are occasionally isolated from each other (Fig. 4B). Under PLM, curved growth lines are visible on the SEUs of several ootaxa (Fig. 4, A to C, and figs. S2 and S6), and the growth lines are distributed throughout the eggshells. In the ootaxa without clear growth lines in PEUs, the SEUs also do not have clear growth lines (Fig. 4D and figs. S3 to S5). In the SEM images, the SEUs are composed of wedges and nucleation centers for the *Faveoloolithus*, *Parafaveoloolithus*, and *Placoolithus* eggshells (Fig. 4, E and F, and fig. S3A). Horizontal grooves left by the degradation of organic fibers are present in the SEUs of the *Placoolithus* eggshells (Fig. 4F), which are comparable to those of the modern avian eggshells (fig. S7). The IPF Y maps show that the *c* axis of the calcite grains of the SEUs is radially arranged around the nucleation center and is parallel to the eggshell growth direction in the outer portion (Fig. 4G). The BC + GB map shows that the SEUs have low- to high-angle grain boundaries and that the SEUs are composed of textured grayscales, but the epitaxial outer diagenetic calcite has a plain grayscale (Fig. 4H). The KAM maps show that the textured grayscale regions of the BC maps have high KAM values (Fig. 4, H and I).

In some cases, SEUs are packed together and form a layer. New pore canals appear above the layer and create a bush-like structure (figs. S3, B to D, S4B, and S5). There is a gap between the layer of SEUs and the underlying PEUs. Isolated small spherical SEUs fill this gap (Fig. 4, J to L, and fig. S3D). In other cases, the SEUs fill the pore canals and extend in every direction because there is no space limitation

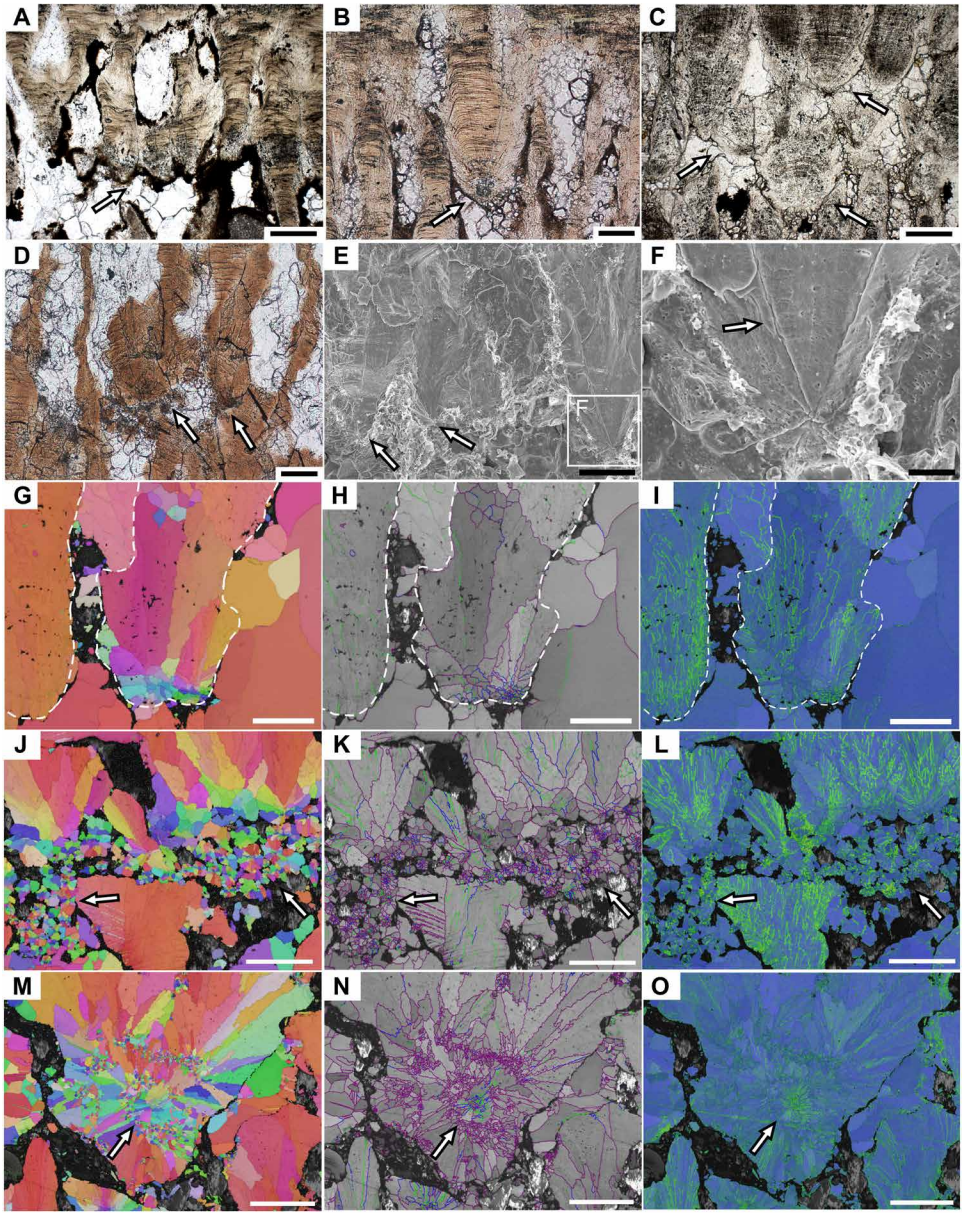

Fig. 4. SEUs of the highly porous eggshells. (**A** to **D**) Thin sections under normal light. (A to C) *Placoolithus* eggshell (TML 4) showing (A) a group of and (B) isolated SEUs (arrows) growing from the cavities between the PEUs, and (C) superimposed SEUs. Note the growth lines on the SEUs. (D) *Parafaveoloolithus* eggshell (IVPP V16857). Note the lack of a clear growth line on the SEUs. (**E** and **F**) SEM images. (E) *Placoolithus* eggshell (TML 4) showing several SEUs (arrows) in the middle part of the eggshell. (F) Enlargement of an SEU in (E), showing the nucleation center, wedges, and horizontal grooves (arrow). (**G** to **I**) SEUs of *Placoolithus* eggshell (TML 4). The dashed lines indicate the boundaries between the eggshell units and abiogenic calcite. (**J** to **L**) A layer of SEUs near the outer surface of the *Youngoolithus* eggshell (IVPP V5783) showing the numerous small spherical SEUs (arrows). (**M** to **O**) A large block of SEUs in the *Youngoolithus* eggshell (IVPP V5783) showing the circular nucleation center (arrows). Note that the straight green line in (O) is an artifact made by a scratch. [(G), (J), and (M)] IPF Y, [(H), (K), and (N)] BC + GB, and [(I), (L), and (O)] KAM maps. Scale bars, 200 μm [(A) and (C)], 100 μm [(B), (D), (E), and (G) to (O)], and 25 μm (F).

for growth. An extreme example is the blocky SEU with a circular nucleation center in the *Youngoolithus* eggshells (Fig. 4, M to O, and fig. S5C).

Moderately porous eggshells

The moderately porous eggshells include four ootaxa: *Megaloolithus*, *Paraspheroolithus*, Stalicoolithidae, and *Stromatoolithus*, whose pore canals are less developed compared with those of the highly porous ootaxa (see figs. S8 and S9, A to I, for additional images). The SEUs are small and usually embedded in PEUs and other larger SEUs or are distributed in pore canals (Fig. 5, A to D). Many of the pore canals are blocked by SEUs in the outer portion of the eggshells (Fig. 5D). Under PLM, curved growth lines are visible on the SEUs of all of these ootaxa (Fig. 5, A to C). The SEM image of the *Megaloolithus* eggshell shows that the SEUs are composed of wedges with curved growth lines and nucleation centers (Fig. 5E), resembling those of *Placoolithus* (Fig. 4F). By contrast, the SEUs of the stalicoolithid

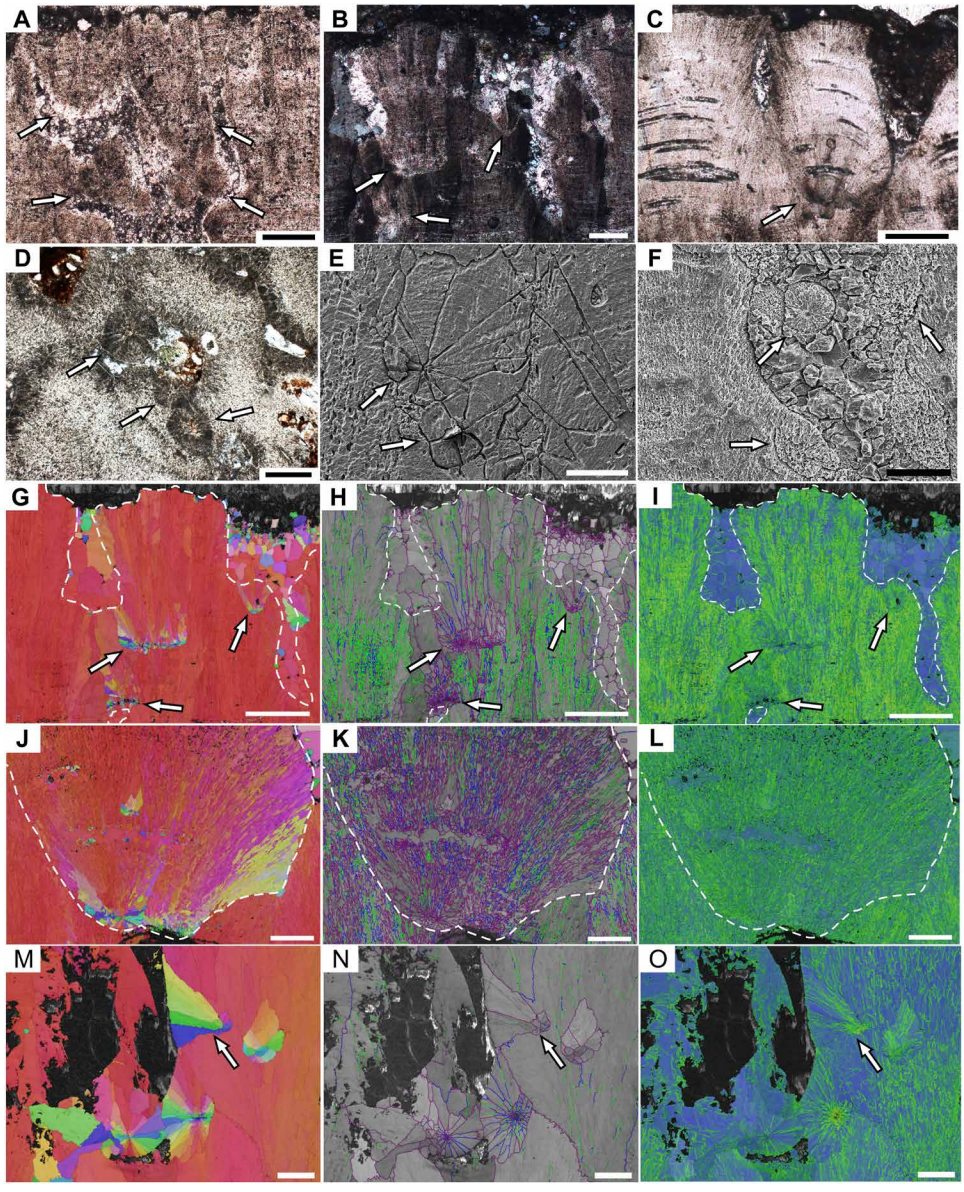

Fig. 5. SEUs of the moderately porous eggshells. (**A** to **D**) Radial thin sections under normal light (A and C), cross-polarized light (B), and a tangential section under normal light (D). The outer portion of the stalicoolithid eggshell (ZMNH M8102) shows SEUs with growth lines (A) in a pore canal (arrows) and (B) embedded in PEUs (arrows). (C) Outer portion of the stalicoolithid eggshell (ZMNH M8929), showing a fan-shaped SEU with growth lines embedded in a PEU (arrow). (D) Stalicoolithid eggshell (ZMNH M8929) showing the SEUs blocking pore canals (arrows). (**E** and **F**) SEM images. (E) *Megaloolithus* eggshell (IVPP V31358) showing SEUs with a nucleation center, wedges, and growth lines (arrows). (F) Stalicoolithid eggshell (TTM 29), showing SEUs with acicular calcite crystals near and inside a pore canal (arrows). (**G** to **I**) EBSD maps of (B). Note that the *c* axis of the SEUs is parallel to the eggshell's growth direction (arrows), and the low-angle grain boundaries and high KAM values of the SEUs. (**J** to **L**) EBSD maps of the fan-shaped SEU shown in (C). (**M** to **O**) EBSD maps of the *Megaloolithus* eggshell (IVPP V31358). The arrows indicate an SEU growing at an angle to the eggshell's main growth direction. The dashed lines in (G) to (I) and (J) to (L) indicate the boundaries between the SEUs and abiogenic calcite, and the contour of the fan-shaped SEU, respectively. [(G), (J), and (M)] IPF Y, [(H), (K), and (N)] BC + GB, and [(I), (L), and (O)] KAM maps. Scale bars, 200 μm [(A) to (D) and (F)], 100 μm [(E) and (M) to (O)], 300 μm [(G) to (I)], and 50 μm [(J) and (K)].

eggshells are composed of acicular calcite crystals and a round nucleation center (Fig. 5F).

The IPF Y maps show that the *c* axis of the calcite grains in most of the SEUs is radially arranged around the nucleation center and is parallel to the eggshell growth direction in the outer portion (Fig. 5, G and J). However, a few of them, especially those near the pore canals, grow at an angle to the eggshell's main growth direction (Fig. 5M). On the BC + GB map, the SEUs, with exposed nucleation centers, have low- and high-angle grain boundaries (Fig. 5, H, K, and N). On the KAM map, the PEUs and SEUs have high KAM values (Fig. 5, I, L, and O).

Oligo-porous eggshells

The eggshell of *Ovaloolithus* is composed of an inner layer with prismatic microstructures and an outer layer with fan-shaped micro-

structures, which are generally similar to those of avian eggshells (fig. S9J). The pore canals are straight and rare and are much less abundant than those in the other dinosaur eggshells analyzed in this study. In one thin section, SEUs with radially arranged calcite crystals occur among the fan-shaped microstructures in the middle portion of the eggshell (fig. S9K), and a group of SEUs is present in a cavity in the outer portion of the eggshell (fig. S9L).

SEUs in turtle and crocodile eggshells

Eggshells of modern turtles *Astrochelys*, *Chelydra*, and *Chelonia*, fossil turtle eggshells of *Testudoolithus* (Fig. 6), and modern crocodile eggshells of *Caiman* (Fig. 7) were analyzed for comparison of the SEUs of the turtle, crocodile, and dinosaur eggshells. The PLM and SEM images reveal that the SEUs of turtle eggshells are composed of an organic core and radially arranged aragonite crystals and are usually

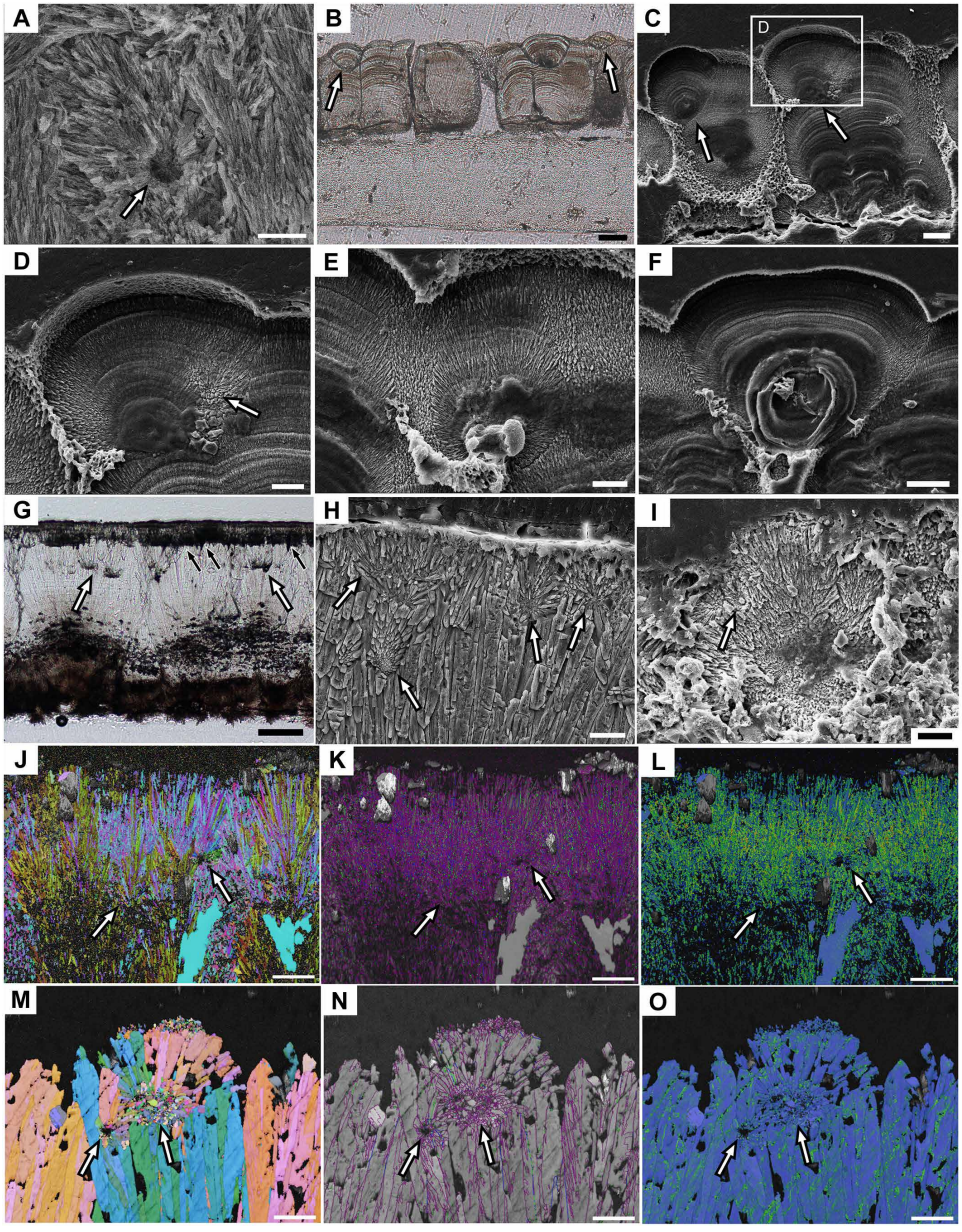

Fig. 6. SEUs of fossil and modern turtle eggshells. (**A**) SEM image of *T. zelenitskyae* eggshell (MOR 710) showing the nucleation center (arrow). (**B** to **F**) *C. serpentine* eggshell. (B) PLM image of the radial thin section. Note that some of the SEUs do not have clear organic cores (arrows). (C) SEM image, showing the SEUs with large organic cores (arrows). (D) Enlargement of the SEU in (C). The arrow indicates a smaller additional eggshell unit embedded in the SEU (tertiary eggshell unit). (E) Enlargement of a couple of SEUs, showing the organic cores connected to the membranes between the aragonite crystals. (F) Enlargement of an SEU between two PEUs. Note the circular membranes surrounding the organic core. (**G** and **H**) *A. radiata* eggshell. (G) PLM image of the radial thin section under normal light. Note the dark layer of SEUs near the outer surface (black arrows) and the isolated SEUs (white arrows). (H) SEM image, showing the SEUs near the outer surface (arrows). (**I**) An eggshell unit of *C. mydas* eggshell. Note the small SEU embedded in the PEU (arrow). (**J** to **L**) EBSD maps of *T. zelenitskyae* eggshell and (**M** to **O**) *A. radiata* eggshell. The arrows indicate the SEUs. Note the radially arranged aragonite grains, dominant high-angle boundaries, and high KAM values of the SEUs. [(J) and (M)] Euler, [(K) and (N)] BC + GB, and [(L) and (O)] KAM maps. Scale bars, 10 μm [(A), (D), (E), and (I)], 50 μm (B), 20 μm [(C), (F), (H), and (M) to (O)], and 100 μm [(G) and (J) to (L)].

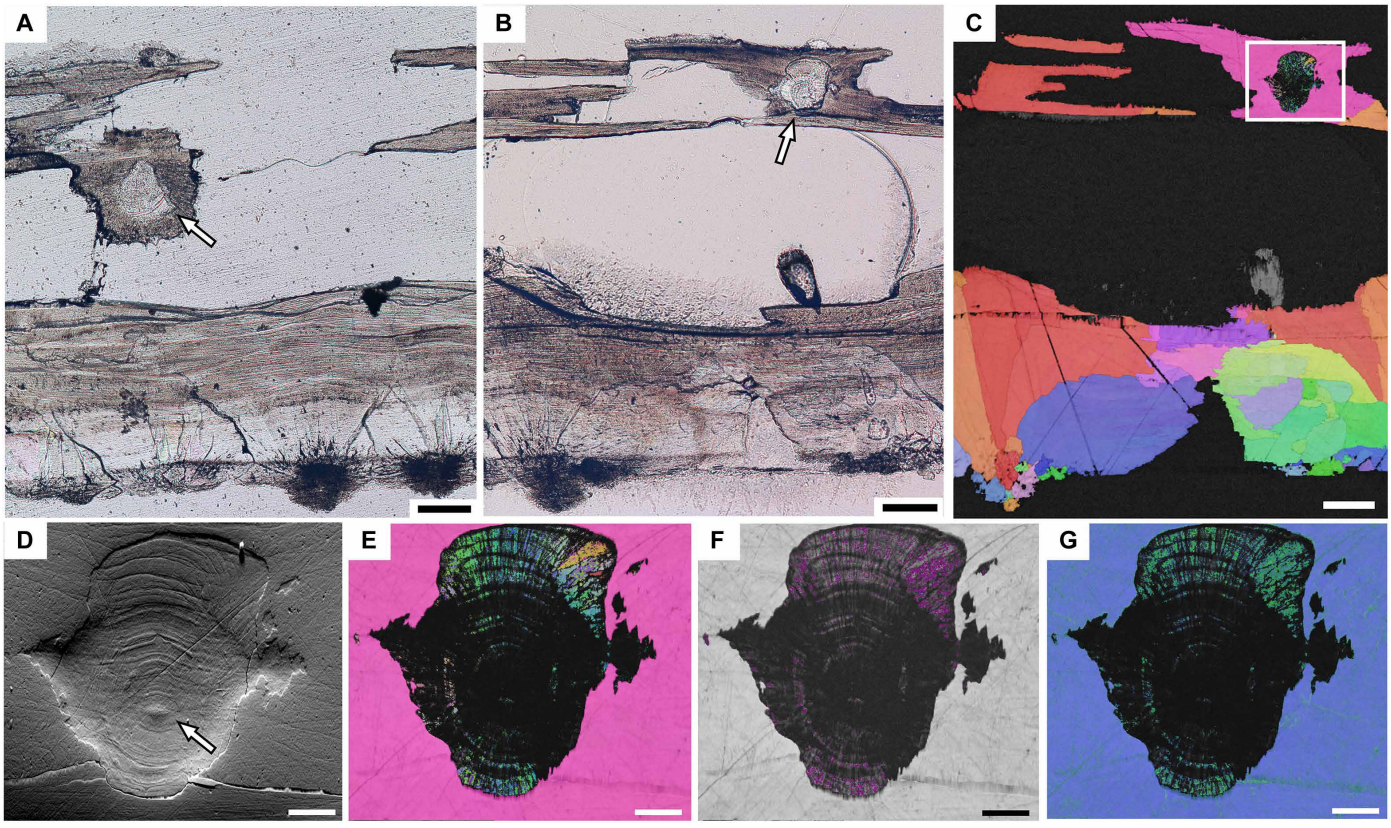

Fig. 7. SEUs of modern crocodile eggshells. (**A** and **B**) PLM image of *C. crocodilus* eggshells, showing the SEUs (arrows) embedded in the PEUs. (**C**) IPF Y map of (B). The white square indicates the SEU shown in (D) to (G). (**D**) SEM image of the SEU. Note that the SEU has a clear organic core (arrow) and concentric growth lines. (**E**) IPF Y map of (D). Note that the *c* axis of the SEU is perpendicular to the eggshell's main growth direction. (**F**) BC + GB and (**G**) KAM maps of (D), showing the high-angle grain boundaries and high KAM values of the SEU, respectively. Scale bars, 100 μm [(A) to (C)] and 20 μm [(D) to (G)].

located near the outer surface of the eggshell (Fig. 6). A few SEUs that do not contain organic cores are also present in a radial thin section (Fig. 6B). Most of the SEUs in the modern turtle eggshells are embedded in PEUs, which is similar to the moderately porous dinosaur eggshells. Distinct growth lines can be observed throughout the SEUs of the *Chelydra* eggshells under PLM and SEM (Fig. 6, B to F). A small SEU is present inside a larger SEU (Fig. 6D). The SEUs of the *Astrochelys* eggshells are relatively small and form layers in the outer portion of the eggshell (Fig. 6, G and H). The SEUs of the *Chelonia* eggshells are very small (Fig. 6I). They are similar to the small SEUs in the *Chelydra* eggshell (Fig. 6D). The Euler maps show that the aragonite grains of the SEUs are radially arranged around the nucleation center (Fig. 6, J and M). The BC + GB map shows that the SEUs have low- and high-angle grain boundaries, and are dominated by high-angle grain boundaries as in adjacent PEUs (Fig. 6, K and N). The KAM map shows that the SEUs have high KAM values (Fig. 6, L and O) (see Supplementary Text for more details of SEUs in turtle eggshells).

The PLM and SEM images reveal that the SEUs of the crocodile eggshell are embedded in the PEUs and are composed of an organic core, circular growth lines, and radially arranged calcite crystals (Fig. 7, A, B, and D). The IPF Y maps show that the calcite grains of the SEUs are radially arranged around the nucleation center and the *c* axis is perpendicular to the eggshell growth direction in the outer portion (Fig. 7, C and E). The BC + GB and KAM maps show that the SEU is dominated by high-angle grain boundaries (Fig. 7F) and high KAM values (Fig. 7G), respectively, consistent with the features of dinosaurian SEUs.

DISCUSSION

Biogenic origin of SEUs in dinosaur eggshells

The results of the combined approach adopted in this study support the hypothesis of a biogenic origin of the SEUs in various ways. First, the SEM images show that the SEUs are composed of wedges or acicular calcite, which resemble the structures of the PEUs. Some SEUs also have small and round nucleation centers (organic core) (Figs. 4, B and F, and 5, E and F). In addition, the porous calcite and horizontal grooves of the SEUs under TEM and SEM, respectively (Figs. 3, I to K, and 4F), indicate that the SEUs contained organic matter (e.g., matrix fibers).

Second, the horizontal and concave-down growth lines under PLM are present throughout the eggshells, including the SEUs (*22*), suggesting that the SEUs and adjacent PEUs grew simultaneously during the biomineralization process. In summary, the SEM, TEM, and PLM observations provide evidence that contradicts earlier research results, which argue that the lack of organic cores and fewer inclusions of organic matter in SEUs suggest a diagenetic origin for the SEUs (*16*).

Third, under EBSD, there is no major difference between the SEUs and PEUs, but the SEUs and abiogenic calcite exhibit considerable differences (Figs. 3 to 5). In the *Megaloolithus* eggshells, as pointed out by Moreno-Azanza *et al.* (*16*), the SEUs

sometimes grow at an angle to the PEU growth direction in the lateral parts of the PEUs. Despite the different growth directions, the presence of growth lines, nucleation centers, textured grayscale on the BC + GB map, and high KAM values suggest that the SEUs are biogenic structures (Fig. 5, N and O, and fig. S8, A, I, and J), and lateral growth toward the empty space between eggshell units is possible during biomineralization, which can also be seen in the biomineralization of the PEUs (Fig. 2). Moreno-Azanza *et al.* (*16*) also pointed out that the SEUs of the *Megaloolithus* eggshells have fewer low-angle grain boundaries compared with the PEUs. However, in contrast to the low-angle grain boundaries, the areas with a textured grayscale on the BC + GB map and high KAM values are more consistent with the areas with growth lines, which are strong signs of the occurrence of biogenic parts in the eggshells (see Supplementary Text for more details). All of the SEUs of the *Megaloolithus* eggshells analyzed in this study and the *Megaloolithus* eggshells analyzed by Moreno-Azanza *et al.* (*16*) have a textured grayscale on the BC + GB map and high KAM values, similar to those of the PEUs (Fig. 5, M to O, and figs. S8 and S10). Thus, we alternatively suggest that the different biomineralization mechanisms of the SEUs and PEUs can potentially explain the dominant high-angle grain boundaries in the SEUs of the *Megaloolithus* eggshells.

Fourth, the consistency of the CL luminescence characteristics of the SEUs and adjacent PEUs suggests that both experienced concomitant taphonomic effects (Fig. 3, L to N, and fig. S1), which refutes the hypothesis that SEUs were formed as a consequence of diagenesis. In addition, previously published CL images of SEUs show that SEUs and PEUs usually have similar brightnesses (*16*, *29*), which is sensibly explained by a contemporaneous origin of the SEUs in relation to the PEUs. Notably, a CL image captured by Moreno-Azanza *et al.* (*16*) shows that the SEUs have luminescence characteristics similar to those of abiogenic calcite, and several abiogenic calcite grains have different luminescence characteristics. This means that CL images only show the combined effect of CL activators and quenchers (*37*), so it may be difficult to identify biogenic and abiogenic parts of fossil eggshells via CL analysis alone without analyzing the element composition. It is worth mentioning that the contents of the nine elements analyzed by Kim *et al.* (*26*) are not different for the PEUs and SEUs, indicating that the SEUs have a similar origin compared to the PEUs.

As a final note, we emphasize that the SEUs of the dinosaur, turtle, and crocodile eggshells are similar in terms of the presence of an organic core, growth lines, and high KAM values, supporting a biogenic origin for the SEUs in the dinosaur eggshells. However, the different mineral compositions of dinosaur and turtle eggshells (aragonite in turtle eggshells) and independent acquisition of fully calcified eggshells of dinosaurs, turtles, and crocodiles (*38*, *39*) indicate that their SEUs are not homologous compared with each other. Dinosaurs, turtles, and crocodiles may have been exposed to similar reproductive selection pressure, which yielded convergent biomineralization processes for the deposition of eggshells. See also Supplementary Text for the additional comparison between the SEUs and the biotically influenced spherulites.

Possible functions of SEUs

Although double-layered eggshells were considered pathological in previous studies (*13*, *30*, *32*), the SEUs in dinosaur, turtle, and crocodile eggshells do not form an additional layer on the outer surface of the original eggshell layer. The universal existence of the SEUs in the eggshells with normal thicknesses indicates that they are probably normal structures in archelosaur eggshells. Because of the prevalent qualitative and quantitative diversity of SEUs among dinosaurs, turtles, and crocodiles, it is reasonable to assume that these structures evolved functions to increase evolutionary fitness. We hypothesize that (i) fully developed SEUs, sizes and shapes similar to those of PEUs, could strengthen the eggshell's mechanical properties and prevent an embryo from external damage and (ii) SEUs in the pore canals could reduce the gas conductance of the eggshells, thus preventing an embryo from drying out. However, the small SEUs embedded in the PEUs or other SEUs probably had little function because other eggshell units replaced them.

In addition, the SEUs may compensate for abnormally halted PEU growth. The layers of numerous small SEUs indicate that there was an organic matrix containing nucleation centers above the PEUs, and the underlying PEUs stopped growing before the formation of the layer of SEUs (Fig. 4, J to L, and fig. S3D). When the PEUs stopped growing for unknown reasons, the SEUs resumed mineralization, forming layers or blocks inside the eggshells (Fig. 4, M to O). Compared with the moderately porous and oligo-porous eggshells, this possible pathological phenomenon was more common in the highly porous eggshells, suggesting that the control capacity of the biomineralization in the highly porous eggshells may have been weaker than that in the other eggshells. Thus, the formation of PEUs could be replaced by the formation of SEUs during the growth of the highly porous eggshells.

Organic control of *c*-axis orientation in porous dinosaur eggshells challenges the competition hypothesis

The crystallography of porous dinosaur eggshells provides a chance to broaden the understanding of eggshell deposition, which has mainly been studied in modern avian eggshells. The consistent outward *c*-axis orientation of the columnar layer of avian eggshells has been suggested to result from a competition between adjacent eggshell units: The crystals radiate from the organic cores in the cone layer and then compete for growth space. Only the crystals with a *c* axis perpendicular to the surface of the eggshell survive and form a columnar layer (*10*, *40*, *41*). However, the highly porous dinosaur eggshells do not support this mode of formation (figs. S2 to S6 and S11). For example, the PEUs of the dictyoolithid eggshells are isolated from each other, and there are large cavities between the PEUs (Fig. 3, A to D, and fig. S11A). Thus, there is no need for competition for space between the PEUs. The SEUs are superimposed on the PEUs or are entirely present inside the cavities, and thus, there is also little competition between the SEUs. However, the IPF Y maps show that the *c* axes of both the PEUs and SEUs of the dictyoolithid eggshell were perpendicular to the surface of the eggshell even in the early stage of their development (Fig. 3B and fig. S4, E and H), suggesting that the consistent *c*-axis direction of the highly porous dinosaur eggshells is probably due to the control of organic matter, rather than competition between the eggshell units. This implies that the competition hypothesis used to explain the crystallography of modern avian eggshells (*42*) may not be successfully applicable to the case of dinosaur eggshells.

By contrast, most of the SEUs of moderately porous dinosaur eggshells are embedded in the PEUs, and they are not restricted to the locations more exposed to dissolution (contra *16*). The fully developed SEUs are only present near the outer surface of the eggshell (Fig. 5, B, C, and G to L, and fig. S8, A, B, and E to G). A similar phenomenon was also observed in the turtle eggshells (Fig. 6, C and

D). Thus, it appears that competition existed between the PEUs and SEUs of the moderately porous dinosaur eggshells due to the limited growth space. The *c*-axis direction of the SEUs deep inside the PEUs or other SEUs is oriented parallel to those of the surrounding PEUs or SEUs. The transverse growth of the crystals in such SEUs was hindered (Fig. 5G and figs. S8K and S9D). Concerning the SEUs in the lateral portion of the PEUs, only the crystals growing toward the center of the PEUs were terminated (Fig. 5M and fig. S8H). Hence, the *c*-axis direction of these two SEUs reflects the growth direction of the surrounding PEUs or SEUs.

Formation mechanism of SEUs

The documented SEUs are explained by potential growing mechanisms to elucidate the dinosaur paleobiology further. On the basis of the microstructure of the highly porous eggshells and the SEUs inside the pore canals of the moderately porous eggshells, it is reasonable to infer that the pore canal system and the cavities between the eggshell units (fig. S11) were filled with uterine fluid containing organic matter (Fig. 8), which controlled the biomineralization (*42*). We hypothesize that the organic matter in the highly and moderately porous eggshells can be divided into two types: One is related to the formation of the eggshell units (biomineralization) (*10*, *43*, *44*), and the other is related to the formation of the pore canals and cavities (non-biomineralization). When the two types of organic matter were secreted simultaneously systematically, the eggshell units, pore canals, and cavities could be organized relative to one another. In some cases, the pore canals and cavities could be partially filled with organic matter related to the biomineralization, and thus, the SEUs formed inside the pore canals and cavities (Fig. 8, A to C). When the growth of the PEUs was interrupted for unknown reasons, the organic matter related to the biomineralization was secreted above the PEUs that had stopped growing, forming numerous nucleation centers and resulting in the formation of a new layer or group of SEUs (Fig. 8, D to F).

Zhao (*11*, *20*) suggested that the eggshell formation mechanism of the eggshells with superimposed SEUs is comparable to that of tuatara (*Sphenodon punctatus*) (*45*, *46*): The eggshell units and the fibers of the shell membrane form simultaneously (Fig. 1, H to J). Nucleation centers form repeatedly on the outer surface of the shell membrane and produce SEUs. However, the shell membrane of the archosaur eggshell is located on the inner surface of the calcareous layer. The fossilized shell membranes preserved in the *Youngoolithus* and *Megaloolithus* eggshells show that the nucleation centers of the PEUs are located on the outer surface of the shell membrane, and the shell membrane did not grow into the calcareous layer (fig. S12, A to E), which is similar to the case of the avian eggshell (fig. S12F). By contrast, growth lines are distributed throughout SEUs, including the calcite crystals radiating inward (fig. S8, C and D). This indicates that the growth of SEUs is controlled by matrix fibers (aforementioned organic matter related to biomineralization), rather than the shell membrane fibers. The limited inward growth of the SEUs also indicates that the formation of the matrix fibers may slightly precede the growth of the eggshell units (Fig. 8). The SEUs of the turtle and crocodile eggshells also suggest that an organic core could occasionally form in the calcareous layer (Figs. 6 and 7). In particular, some of them are connected to the matrix between the calcium

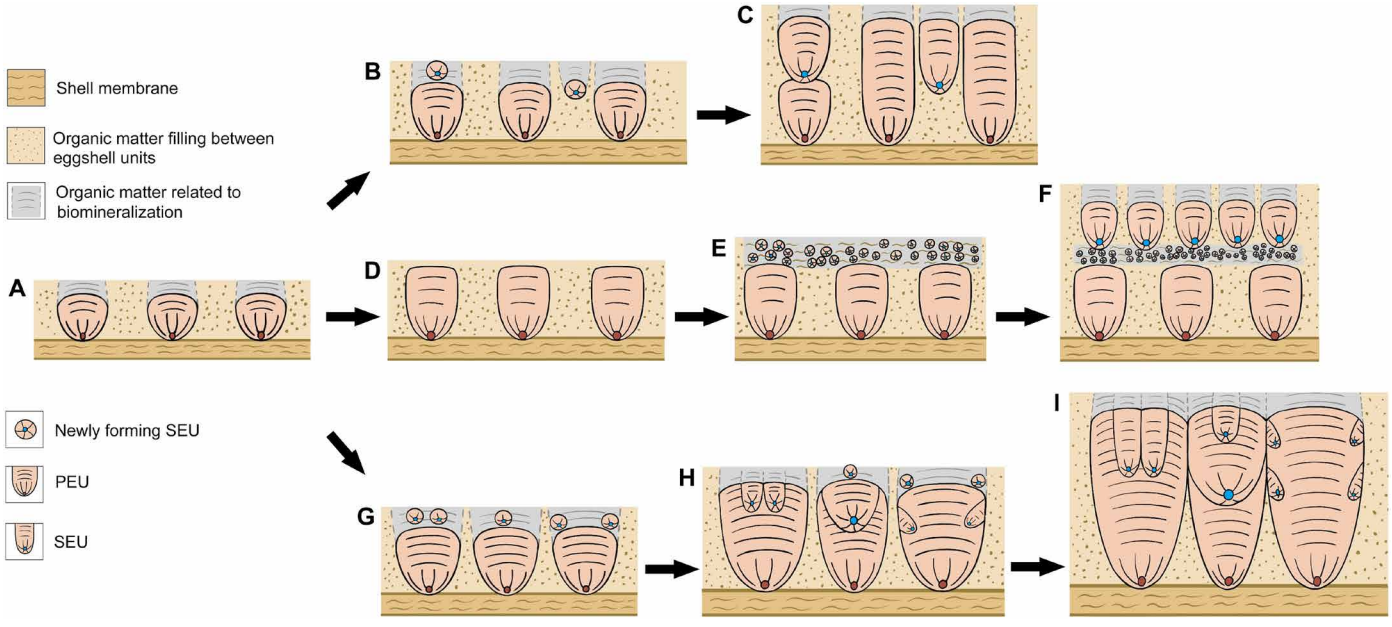

Fig. 8. Formation mechanism of dinosaur eggshells containing SEUs. (**A**) PEUs growing from the organic cores on the shell membrane. (**B** and **C**) Typical case of highly porous eggshells. (B) SEUs growing above the PEUs (left) or from the spaces between the PEUs (right). (C) SEUs continue growing and superimpose on PEUs (left) or occupying the space between the PEUs (right). (**D** to **F**) Possible pathological case of highly porous eggshells. (D) PEUs stop growing. (E) Organic matter related to biomineralization is secreted above the PEUs, and small spherical SEUs form within the organic matter. (F) Some of the small spherical SEUs continue growing, forming a layer of SEUs. (**G** to **I**) Moderately porous eggshells. (G) Because of the limited space between the PEUs, the SEUs grow above the PEUs. (H) Both the PEUs and SEUs continue growing. The PEUs encase the overlying SEUs. The SEUs in the middle portion of the PEU grow outward with the PEU (left). Some of the SEUs are fully developed and replace the underlying PEU (middle). The SEUs in the peripheral portion of the PEU grow toward the lateral edges of the PEU (right). New SEUs form above the SEU (middle) and PEU (right). (I) The PEUs and SEUs continue growing. New SEUs are encased by the SEU (middle) and PEU (right) below them.

carbonate crystals, rather than to the fibers of the shell membrane (Fig. 6, E and F).

In summary, the shell membrane fibers of the dinosaur eggshells are restricted to the inner surface of the calcareous layer and do not form simultaneously with the eggshell units. The similarities between the SEUs of dinosaur, turtle, and crocodile eggshells reveal that the formation mechanism of the dinosaur eggshells containing SEUs is comparable to those of turtle and crocodile eggshells, rather than that of *S. punctatus* eggshells.

Evolution and loss of SEUs in dinosaur eggshells

The biogenic origin of SEUs provides an unexplored opportunity to trace the evolution of the SEUs. The recent findings regarding dinosaur eggshells with minimal mineralization provide additional support for the hypothesis that suggests that the most recent common ancestor of all dinosaurs laid poorly mineralized eggs, and well-mineralized eggs were independently developed by theropods, sauropods, and ornithischian dinosaurs (*47*–*49*). In addition to Dinosauria, some turtles and all crocodiles also independently developed highly calcified eggshells (*38*, *39*). SEUs can form only after eggshells acquire sufficient mineralization, so it is reasonable to infer that SEUs were independently developed by turtles, crocodiles, and dinosaur clades with fully calcified eggshells (Fig. 9A).

The current understanding of egg layers of dinosaur eggshells containing SEUs is very limited. The only definite clades are titanosaurs and hadrosaurs, which laid Megaloolithidae (*27*, *28*) and *Stromatoolithus* (*50*), respectively. Moreover, highly porous eggshells similar to the materials analyzed in this study have been either inferred to be sauropods (*51*, *52*) or confirmed to be basal tetanuran eggshells (*53*), while the moderately porous eggshells have been inferred to be hadrosaurs (*50*). Thus, in a conservative view, only ornithischian and sauropod eggshells had SEUs, but if at least one eggshell analyzed in this study was laid by basal tetanuran dinosaurs (*53*), then the tetanuran dinosaurs can be included as an additional clade that had SEUs. Consequently, it can be inferred that the SEUs of eggshells laid by turtles, crocodiles, ornithischians, sauropods, and tetanurans have independent origins and thus are not homologous with one another (i.e., homoplasy) (Fig. 9A). Furthermore, considering the near absence of SEUs in maniraptoran (including modern bird) eggshells (*30*), it appears that the biomineralization

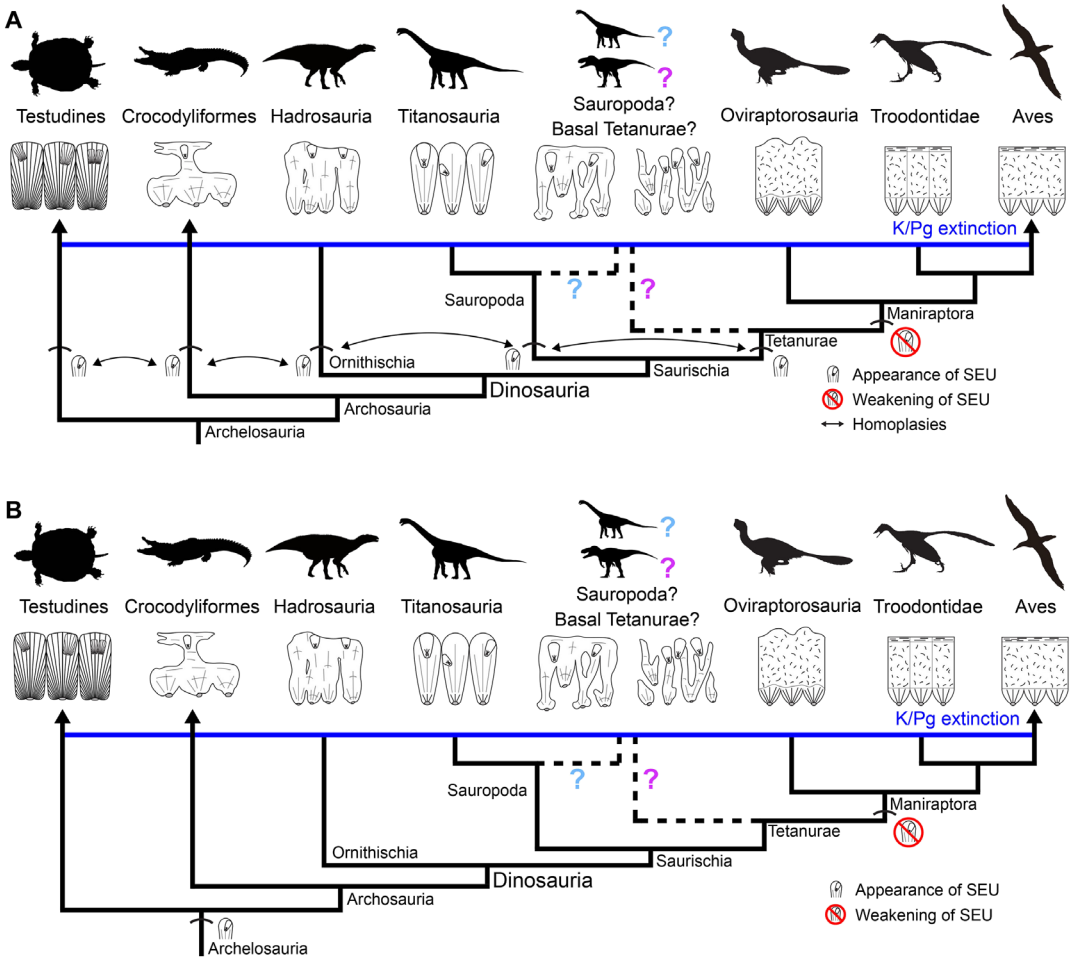

Fig. 9. The evolution of the SEUs. (**A**) The SEUs present in eggshells of turtles, crocodiles, ornithischian, titanosaurian, and potentially in basal tetanuran dinosaurs are homoplastic to one another but became very rare among the maniraptoran eggshells, which may have been influenced by their physiological changes. (**B**) The alternative (parsimonious) scenario based on the assumption that the appearance of SEUs is related to a deep homology (*54*) among archelosaurs and the common presence of SEUs indicate parallel evolution. The question marks and dashed lines indicate the uncertainty of the egg layer information of the highly porous eggshells. The silhouettes of the Troodontidae and Oviraptorosauria are from Phylopic (http://phylopic.org; by S. Hartman and E. Willoughby, respectively).

mechanism (or control) of dinosaur eggshells changed near the cladogenesis of Maniraptora (Fig. 9A).

Alternatively, the appearance of SEUs might have been deeply rooted in archelosaur evolution [i.e., deep homology sensu (*54*)], so the seemingly homoplastic appearance of SEUs in archelosaur eggshells may be interpreted as parallel evolution (*54*, *55*) (Fig. 9B). Although this scenario is less likely, it provides a more parsimonious explanation for the appearance and disappearance of SEUs in archelosaur eggshells (Fig. 9B).

Regardless of which of the two scenarios is closer to the truth, the evolution of SEUs offers a glimpse of the physiological evolution of dinosaurs. The presence of SEUs in a wide taxonomic range of Archelosauria (Fig. 9) implies that starting a new mineralization (SEUs) during the ongoing mineralization process was prevalent and the controlled secretion of an organic matrix during biomineralization may not have been strict enough to prevent the formation of SEUs. By contrast, modern avian eggshells are characterized by precise temporal and spatial control of the sequential secretion of matrix proteins, resulting in the formation of at least two different eggshell layers (*41*). Experimental studies have demonstrated that the types of dominant matrix proteins formed during the initial (cone layer deposition) and mature (columnar layer deposition) stages of avian eggshell biomineralization are different (*10*, *43*, *44*). In addition, the quantity and diversity of these matrix proteins notably increase toward the mature stage of biomineralization (*43*, *44*), meaning that the effects of the biomineralization initiator, which may cause SEUs to form during the ongoing biomineralization process, may be very minimal in the case of maniraptoran dinosaur eggshells containing multiple sublayers. Most non-maniraptoran dinosaur eggshells characterized by the presence of SEUs are composed of a single layer. In this case, the secretion of an initiator may have been more frequent and not interrupted by a much more dominant matrix protein, which is unfavorable for the formation of SEUs (as in the case of maniraptoran eggshells). Thus, the deposition of new SEUs may have been more feasible in non-maniraptoran dinosaur eggshells.

In summary, the biomineralization of maniraptoran eggshells would have been more organized not only regarding the fossilizable microstructure but also for non-fossilizable physiological mechanisms such as matrix protein secretions. The synapomorphic microstructure of maniraptoran eggshells and its underlying physiological process would have affected the disappearance of SEUs (Fig. 9), which is still the status quo for modern avian eggshells (*33*).

MATERIALS AND METHODS

Histology

All of the eggshell fragments were embedded in EXAKT Technovit 7200 one-component resin. Radial and tangential thin sections were prepared using an EXAKT 300CP and EXAKT 400CS cutting and grinding system (housed at IVPP). The thickness of the thin sections was about 40 μm. The thin sections were viewed and photographed under PLM using a Zeiss Axio Imager A2 (housed at IVPP).

SEM analysis

The radial thin sections of the *Faveoloolithus*, *Megaloolithus*, *Parafaveoloolithus*, *Stalicoolithus*, *Testudoolithus*, and *Astrochelys* eggshells were polished using P4000 sandpaper and etched using acetic acid (5%) for 8 min, 3 min, 7 min, 7 min, 2 min, and 30 s, respectively. The radial sections of the *Chelydra*, *Chelonia*, and *Dromaius* eggshells were polished and etched using hydrochloric acid (1%) for 4 s, 4 s, and 40 s, respectively. All of the specimens were coated with gold. The *Faveoloolithus* eggshell thin section was viewed under an FEI FEG 650 SEM [housed at Peking University (PKU)]. The *Megaloolithus*, stalicoolithid, *Testudoolithus*, *Chelydra*, *Chelonia*, and *Dromaius* eggshell thin sections were viewed under a Zeiss MA EVO25 SEM (housed at IVPP). The *Astrochelys* eggshell thin section was viewed under a TESCAN Vega 3 SBH SEM [housed at the SEM Laboratory, School of Earth Sciences, China University of Geosciences (CUG, Wuhan)]. The radially fractured section of the *Placoolithus* and *Struthio* eggshells was etched using hydrochloric acid (1%) for 15 s and 5 s, respectively, and then coated with gold and viewed under a Hitachi S-3700N SEM (housed at IVPP) (see Supplementary Text for more details).

The *Caiman* eggshell was not etched but very well-polished as in usual EBSD specimens. The sample was carbon-coated, and the fore-scattered image was captured by the EBSD detector (Oxford Instruments Symmetry), housed at the School of Earth and Environmental Sciences, Seoul National University (SNU).

FIB-SEM and TEM analyses

The sample for TEM analysis was collected from a radial thin section of the *Placoolithus* eggshell. The thin section was polished using a 0.05-μm colloidal silica compound and then observed using a Helios Nanolab G3 FIB-SEM [housed at Utrecht University (UU)]. After choosing the target SEU, the FIB-SEM was used to prepare electron-transparent thin foils (final thickness of <100 nm), and the Pt-coated specimen was analyzed in the secondary electron and backscattered electron modes under high vacuum. The analytical conditions were an accelerating voltage of 2 to 15 kV, a low current of 0.1 nA, and a working distance of 4 mm. Subsequently, the thin foils were analyzed using an FEI Talos F200X STEM (housed at UU) operated at 200 kV.

EBSD analysis

The radial thin sections of the *Faveoloolithus*, *Megaloolithus*, *Multifissoolithus*, *Paraspheroolithus*, *Placoolithus*, *Stromatoolithus*, *Youngoolithus*, dictyoolithid, stalicoolithid, *Testudoolithus*, *Astrochelys* eggshells, and *Caiman* eggshells were further polished using a 0.5-μm diamond compound and then a 0.05-μm colloidal silica. The fossil eggshells were analyzed using the Symmetry detector attached to a JEOL JSM-7100F FE-SEM (housed at SNU) after carbon coating. All of the specimens were analyzed using the Aztec 4.3 software under an acceleration voltage of 15.0 kV and a working distance of 15.0 or 25.0 mm (*56*).

CL analysis

The radial thin sections of the *Faveoloolithus*, *Placoolithus*, *Youngoolithus*, dictyoolithid, and stalicoolithid eggshells were viewed under a Leica DM2700P optical microscope (housed at the Cathodoluminescence and Scanning Microscopy Laboratory, CUG, Wuhan). The CL images were taken using an attached CITL MK5-2 CL instrument. The working conditions were as follows: accelerating voltage of 10 kV, beam current of 250 μA, and low-vacuum mode of 0.003 mbar.

Supplementary Materials

This PDF file includes:

Supplementary Text
Figs. S1 to S12
Table S1
References

REFERENCES AND NOTES

1. A. K. Behrensmeyer, S. M. Kidwell, R. A. Gastaldo, Taphonomy and paleobiology. *Paleobiology* **26**, 103–147 (2000).
2. A. Pérez-Huerta, I. Coronado, T. A. Hegna, Understanding biomineralization in the fossil record. *Earth Sci. Rev.* **179**, 95–122 (2018).
3. K. E. Mikhailov, Fossil and recent eggshell in amniotic vertebrates: Fine structure, comparative morphology and classification. *Spec. Pap. Palaeontol.* **56**, 1–80 (1997).
4. G. Grellet-Tinner, L. Chiappe, M. Norell, D. Bottjer, Dinosaur eggs and nesting behaviors: A paleobiological investigation. *Palaeogeogr. Palaeoclimatol. Palaeoecol.* **232**, 294–321 (2006).
5. Z. Zhao, Q. Wang, S. Zhang, *Dinosaur Eggs* (Palaeovertebrata Sinica, Science Press, 2015).
6. B. Demarchi, J. Stiller, A. Grealy, M. Mackie, Y. Deng, T. Gilbert, J. Clarke, L. J. Legendre, R. Boano, T. Sicheritz-Pontén, J. Magee, G. Zhang, M. Bunce, M. J. Collins, G. Miller, Ancient proteins resolve controversy over the identity of *Genyornis* eggshell. *Proc. Natl. Acad. Sci. U.S.A.* **119**, e2109326119 (2022).
7. R. A. Eagle, M. Enriquez, G. Grellet-Tinner, A. Pérez-Huerta, D. Hu, T. Tütken, S. Montanari, S. J. Loyd, P. Ramirez, A. K. Tripati, M. J. Kohn, T. E. Cerling, L. M. Chiappe, J. M. Eiler, Isotopic ordering in eggshells reflects body temperatures and suggests differing thermophysiology in two Cretaceous dinosaurs. *Nat. Commun.* **6**, 8296 (2015).
8. R. R. Dawson, D. J. Field, P. M. Hull, D. K. Zelenitsky, F. Therrien, H. P. Affek, Eggshell geochemistry reveals ancestral metabolic thermoregulation in Dinosauria. *Sci. Adv.* **6**, eaax9361 (2020).
9. M. Tagliavento, A. J. Davies, M. Bernecker, P. T. Staudigel, R. R. Dawson, M. Dietzel, K. Götschl, W. Guo, A. S. Schulp, F. Therrien, D. K. Zelenitsky, A. Gerdes, W. Müller, J. Fiebig, Evidence for heterothermic endothermy and reptile-like eggshell mineralization in *Troodon*, a non-avian maniraptoran theropod. *Proc. Natl. Acad. Sci. U.S.A.* **120**, e2213987120 (2023).
10. J. Gautron, L. Stapane, N. Le Roy, Y. Nys, A. B. Rodriguez-Navarro, M. T. Hincke, Avian eggshell biomineralization: An update on its structure, mineralogy and protein tool kit. *BMC Mol. Cell Biol.* **22**, 11 (2021).
11. Z. Zhao, "Dinosaur eggs in China: On the structure and evolution of eggshells" in *Dinosaur Eggs and Babies*, K. Carpenter, K. F. Hirsch, J. R. Horner, Eds. (Cambridge Univ. Press, 1994), chap. 12, pp. 184–203.
12. D. K. Zelenitsky, L. V. Hills, Normal and pathological eggshells of *Spheroolithus albertensis*, oosp. nov., from the Oldman Formation (Judith River Group, late Campanian), southern Alberta. *J. Vertebr. Paleontol.* **17**, 167–171 (1997).
13. F. D. Jackson, A. Garrido, J. G. Schmitt, L. M. Chiappe, L. Dingus, D. B. Loope, Abnormal, multilayered titanosaur (Dinosauria: Sauropoda) eggs from in situ clutches at the Auca Mahuevo Locality, Neuquen Province, Argentina. *J. Vertebr. Paleontol.* **24**, 913–922 (2004).
14. A. G. Sellés, B. Vila, À. Galobart, Evidence of reproductive stress in titanosaurian sauropods triggered by an increase in ecological competition. *Sci. Rep.* **7**, 13827 (2017).
15. K. F. Hirsch, "Pathological amniote eggshell—Fossil and modern" in *Mesozoic Vertebrate Life*, D. H. Tanke, K. Carpenter, Eds. (Indiana Univ. Press, 2001), chap. 26, pp. 378–392.
16. M. Moreno-Azanza, B. Bauluz, J. I. Canudo, J. M. Gasca, F. T. Fernández-Baldor, Combined use of electron and light microscopy techniques reveals false secondary shell units in Megaloolithidae eggshells. *PLOS ONE* **11**, e0153026 (2016).
17. M. A. Ewert, S. J. Firth, C. E. Nelson, Normal and multiple eggshells in batagurine turtles and their implications for dinosaurs and other reptiles. *Can. J. Zool.* **62**, 1834–1841 (1984).
18. H. H. Schleich, W. Kästle, *Reptile Egg-Shells SEM Atlas* (Gustav-Fischer Verlag, 1988).
19. R. Kohring, Fossil reptile egg shells (Chelonia, Crocodilia, Dinosauria) from the Lower Barremian of Galve (Province of Teruel, SE Spain). *Paläont. Z.* **64**, 329–344 (1990).
20. Z. Zhao, "Structure, formation, and evolutionary trends of dinosaur eggshell" in *Structure, Formation and Evolution of Fossil Hard Tissues*, I. Kobayashi, H. Mutvei, A. Sahni, Eds. (Tokai Univ. Press, 1993), pp. 195–212.
21. S. Zhang, A parataxonomic revision of the Cretaceous faveoloolithid eggs of China. *Vert. PalAsiat.* **48**, 203–219 (2010).
22. S. Zhang, A revision of the eggshell fragment of *Spheroolithus megadermus* from Laiyang, Shandong Province, China. *Vert. PalAsiat.* **60**, 59–68 (2022).
23. Q. Wang, X. Wang, Z. Zhao, Y. Jiang, A new oofamily of dinosaur egg from the Upper Cretaceous of Tiantai Basin, Zhejiang Province, and its mechanism of eggshell formation. *Chin. Sci. Bull.* **57**, 3740–3747 (2012).
24. Q. Wang, Z. Zhao, X. Wang, S. Zhang, Y. Jiang, New forms of dictyoolithids from the Tiantai Basin, Zhejiang Province of China and a parataxonomic revision of the dictyoolithids. *Vert. PalAsiat.* **51**, 43–54 (2013).
25. S. Zhang, T.-R. Yang, Z. Li, Y. Hu, New dinosaur egg material from Yunxian, Hubei Province, China resolves the classification of dendroolithid eggs. *Acta Palaeontol. Pol.* **63**, 671–678 (2018).
26. N.-H. Kim, S. Choi, S. Kim, Y.-N. Lee, A new faveoloolithid oogenus from the Wido Volcanics (Upper Cretaceous), South Korea and a new insight into the oofamily Faveoloolithidae. *Cretac. Res.* **100**, 145–163 (2019).
27. L. M. Chiappe, R. A. Coria, L. Dingus, F. Jackson, A. Chinsamy, M. Fox, Sauropod dinosaur embryos from the Late Cretaceous of Patagonia. *Nature* **396**, 258–261 (1998).
28. M. Kundrát, R. A. Coria, T. W. Manning, D. Snitting, L. M. Chiappe, J. Nudds, P. E. Ahlberg, Specialized craniofacial anatomy of a titanosaurian embryo from Argentina. *Curr. Biol.* **30**, 4263–4269.e2 (2020).
29. G. Grellet-Tinner, F. Corsetti, A. D. Buscalioni, The importance of microscopic examinations of eggshells: Discrimination of bioalteration and diagenetic overprints from biological features. *J. Iber. Geol.* **36**, 181–192 (2010).
30. M. Vianey-Liaud, P. Mallan, O. Buscail, C. Montgelard, "Review of France dinosaur eggshells: Morphology, structure, mineral and organic composition" in *Dinosaur Eggs and Babies*, K. Carpenter, K. F. Hirsch, J. R. Horner, Eds. (Cambridge Univ. Press, 1994), chap. 11, pp. 151–183.
31. D. M. Mohabey, Systematics of Indian Upper Cretaceous dinosaur and chelonian eggshells. *J. Vertebr. Paleontol.* **18**, 348–362 (1998).
32. F. D. Jackson, J. G. Schmitt, Recognition of vertebrate egg abnormalities in the Upper Cretaceous fossil record. *Cretac. Res.* **29**, 27–39 (2008).
33. F. D. Jackson, D. J. Varricchio, Abnormal, multilayered eggshell in birds: Implications for dinosaur reproductive anatomy. *J. Vertebr. Paleontol.* **23**, 699–702 (2003).
34. S. Choi, Y. Park, J. J. Kweon, S. Kim, H. Jung, S. K. Lee, Y.-N. Lee, Fossil eggshells of amniotes as a paleothermometry tool. *Palaeogeogr. Palaeoclimatol. Palaeoecol.* **571**, 110376 (2021).
35. E. T. Saitta, J. Vinther, M. K. Crisp, G. D. Abbott, L. Wheeler, S. Presslee, T. G. Kaye, I. Bull, I. Fletcher, X. Chen, D. Vidal, F. Sanguino, Á. D. Buscalioni, J. Calvo, P. C. Sereno, S. L. Baumgart, M. Pittman, M. J. Collins, J. Sakalauskaite, M. Mackie, F. Dal Bello, M. R. Dickinson, M. A. Stevenson, P. Donohoe, P. R. Heck, B. Demarchi, K. E. H. Penkman, Non-avian dinosaur eggshell calcite can contain ancient, endogenous amino acids. *Geochim. Cosmochim. Acta* **365**, 1–20 (2024).
36. F. D. Jackson, H. R. Horner, D. J. Varricchio, A study of a *Troodon* egg containing embryonic remains using epifluorescence microscopy and other techniques. *Cretac. Res.* **31**, 255–262 (2010).
37. V. Barbin, Application of cathodoluminescence microscopy to recent and past biological materials: A decade of progress. *Mineral. Petrol.* **107**, 353–362 (2013).
38. P. M. Sander, Reproduction in early amniotes. *Science* **337**, 806–808 (2012).
39. L. J. Legendre, S. Choi, J. A. Clarke, The diverse terminology of reptile eggshell microstructure and its effect on phylogenetic comparative analyses. *J. Anat.* **241**, 641–666 (2022).
40. J. M. García-Ruiz, A. Rodriguez Navarro, O. Kälin, Textural analysis of eggshells. *Mater. Sci. Eng. C* **3**, 95–100 (1995).
41. Y. Nys, J. Gautron, J. M. Garcia-Ruiz, M. T. Hincke, Avian eggshell mineralization: Biochemical and functional characterization of matrix proteins. *C. R. Palevol.* **3**, 549–562 (2004).
42. J. M. Dominguez-Vera, J. Gautron, J. M. Garcia-Ruiz, Y. Nys, The effect of avian uterine fluid on the growth behavior of calcite crystals. *Poult. Sci.* **79**, 901–907 (2000).
43. P. Marie, V. Labas, A. Brionne, G. Harichaux, C. Hennequet-Antier, A. B. Rodriguez-Navarro, Y. Nys, J. Gautron, Quantitative proteomics provides new insights into chicken eggshell matrix protein functions during the primary events of mineralization and the active calcification phase. *J. Proteomics* **126**, 140–154 (2015).
44. N. Le Roy, L. Combes-Soia, A. Brionne, V. Labas, A. B. Rodriguez-Navarro, M. T. Hincke, Y. Nys, J. Gautron, Guinea fowl eggshell quantitative proteomics yield new findings related to its unique structural characteristics and superior mechanical properties. *J. Proteomics* **209**, 103511 (2019).
45. M. J. Packard, K. F. Hirsch, V. B. Meyer-Rochow, Structure of the shell from eggs of the tuatara, *Sphenodon punctatus*. *J. Morphol.* **174**, 197–205 (1982).
46. M. J. Packard, B. T. Michael, N. G. Kenneth, V. Marta, Aspects of shell formation in eggs of the tuatara, *Sphenodon punctatus*. *J. Morphol.* **197**, 147–157 (1988).
47. K. Stein, E. Prondvai, T. Huang, J.-M. Baele, P. M. Sander, R. Reisz, Structure and evolutionary implications of the earliest (Sinemurian, Early Jurassic) dinosaur eggs and eggshells. *Sci. Rep.* **9**, 4424 (2019).
48. M. A. Norell, J. Wiemann, M. Fabbri, C. Yu, C. A. Marsicano, A. Moore-Nall, D. J. Varricchio, D. Pol, D. K. Zelenitsky, The first dinosaur egg was soft. *Nature* **583**, 406–410 (2020).
49. F. Han, Y. Yu, S. Zhang, R. Zeng, X. Wang, H. Cai, T. Wu, Y. Wen, S. Cai, C. Li, R. Wu, Q. Zhao, X. Xu, Exceptional Early Jurassic fossils with leathery eggs shed light on dinosaur reproductive biology. *Natl. Sci. Rev.* **11**, nwad258 (2024).
50. X. Zhu, Q. Wang, X. Wang, Restudy of the original and new materials of *Stromatoolithus pinglingensis* and discussion on some Spheroolithidae eggs. *Hist. Biol.* **34**, 283–297 (2022).
51. G. Grellet-Tinner, V. Codrea, A. Folie, A. Higa, T. Smith, First evidence of reproductive adaptation to "island effect" of a dwarf Cretaceous Romanian titanosaur, with embryonic integument in ovo. *PLOS ONE* **7**, e32051 (2012).
52. M. Kundrát, A. R. I. Cruickshank, New information on multispherulitic dinosaur eggs: Faveoloolithidae and Dendroolithidae. *Hist. Biol.* **34**, 1072–1084 (2022).
53. R. Araújo, R. Castanhinha, R. M. S. Martins, O. Mateus, C. Hendrickx, F. Beckmann, N. Schell, L. C. Alves, Filling the gaps of dinosaur eggshell phylogeny: Late Jurassic theropod clutch with embryo from Portugal. *Sci. Rep.* **3**, 1924 (2013).

54. N. Shubin, C. Tabin, S. Carroll, Deep homology and the origins of evolutionary novelty. *Nature* **457**, 818–823 (2009).
55. B. K. Hall, Descent with modification: The unity underlying homology and homoplasy as seen through an analysis of development and evolution. *Biol. Rev.* **78**, 409–433 (2003).
56. S. Choi, Y. Park, M. Moreno-Azanza, Protocol for electron backscatter diffraction (EBSD) analysis of fossil eggshells. *J. Vertebr. Paleontol.* **43**, e2363210 (2024).
57. L. Xu, J. Xie, S. Zhang, S. Choi, N.-H. Kim, D. Gao, X. Jin, S. Jia, Y. Gao, Fossil turtle eggs from the Upper Cretaceous Gaogou Formation, Xiaguan-Gaoqiu Basin, Neixiang County, Henan Province, China: Interpretation of the transformation from aragonite to calcite in fossil turtle eggshell. *Cretac. Res.* **314**, 105116 (2022).
58. J. Aizenberg, J. Hanson, T. F. Koetzle, S. Weiner, L. Addadi, Control of macromolecule distribution within synthetic and biogenic single calcite crystals. *J. Am. Chem. Soc.* **119**, 881–886 (1997).
59. Y.-Y. Kim, J. D. Carloni, B. Demarchi, D. Sparks, D. G. Reid, M. E. Kunitake, C. C. Tang, M. J. Duer, C. L. Freeman, B. Pokroy, K. Penkman, J. H. Harding, L. A. Estroff, S. P. Baker, F. C. Meldrum, Tuning hardness in calcite by incorporation of amino acids. *Nat. Mater.* **15**, 903–910 (2016).
60. Y. Nys, M. T. Hincke, J. L. Arias, J. M. Garcia-Ruiz, S. E. Solomon, Avian eggshell mineralization. *Poult. Avian Biol. Rev.* **10**, 143–166 (1999).
61. D. Athanasiadou, W. Jiang, D. Goldbaum, A. Saleem, K. Basu, M. S. Pacella, C. F. Böhm, R. R. Chromik, M. T. Hincke, A. B. Rodríguez-Navarro, H. Vali, S. E. Wolf, J. J. Gray, K. H. Bui, M. D. McKee, Nanostructure, osteopontin, and mechanical properties of calcitic avian eggshell. *Sci. Adv.* **4**, eaar3219 (2018).
62. A. B. Rodríguez-Navarro, N. Domínguez-Gasca, D. Athanasiadou, N. Le Roy, A. González-Segura, N. Reznikov, M. T. Hincke, M. D. McKee, A. G. Checa, Y. Nys, J. Gautron, Guinea fowl eggshell structural analysis at different scales reveals how organic matrix induces microstructural shifts that enhance its mechanical properties. *Acta Biomater.* **178**, 244–256 (2024).
63. A. V. López, S. Choi, Y. Park, D. Hanley, J.-W. Lee, M. Honza, R. E. Bolmaro, Avian obligate brood parasitic lineages evolved variable complex polycrystalline structures to build tougher eggshells. *iScience* **26**, 108552 (2023).
64. R. Mercedes-Martín, M. R. Rogerson, A. T. Brasier, H. B. Vonhof, T. J. Prior, S. M. Fellows, J. J. G. Reijmer, I. Billing, H. M. Pedley, Growing spherulitic calcite grains in saline, hyperalkaline lakes: Experimental evaluation of the effects of Mg-clays and organic acids. *Sediment. Geol.* **335**, 93–102 (2016).
65. R. Mercedes-Martín, A. Rao, M. Rogerson, M. Sánchez-Román, Effects of salinity, organic acids and alkalinity on the growth of calcite spherulites: Implications for evaporitic lacustrine sedimentation. *Depositional Rec.* **8**, 143–164 (2022).
66. H. Chafetz, J. Barth, M. Cook, X. Guo, J. Zhou, Origins of carbonate spherulites: Implications for Brazilian Aptian pre-salt reservoir. *Sediment. Geol.* **365**, 21–33 (2018).
67. S. Wu, J. I. Blake, L. Guo, W. Zhou, Naturally occurring and biomimetic synthesized calcite spherulites. *Cryst. Growth Des.* **20**, 3537–3545 (2020).
68. F. Nindiyasari, E. Griesshaber, L. Fernández-Díaz, J. Manuel Astilleros, N. Sánchez-Pastor, A. Ziegler, W. W. Schmahl, Effects of Mg and hydrogel solid content on the crystallization of calcium carbonate in biomimetic counter-diffusion systems. *Cryst. Growth Des.* **14**, 4790–4802 (2014).
69. Z. Zhao, S. Ding, Discovery of the dinosaur eggs from Alashanzuoqi and its stratigraphical meaning. *Vert. PalAsiat.* **14**, 42–44 (1976).
70. A. G. Sellés, A. M. Bravo, X. Delclòs, F. Colombo, X. Martí, J. Ortega-Blanco, C. Parellada, À. Galobart, Dinosaur eggs in the Upper Cretaceous of the Coll de Nargó area, Lleida Province, south-central Pyrenees, Spain: Oodiversity, biostratigraphy and their implications. *Cretac. Res.* **40**, 10–20 (2013).
71. Z. Zhao, "The advancement of research on the dinosaurian eggs in China" in *Mesozoic and Cenozoic Redbeds in Southern China*, Institute of Vertebrate Paleontology and Paleoanthropology and Nanjing Institute of Geology and Palaeontology, Chinese Academy of Sciences Eds. (Science Press, Beijing, 1979), pp. 330–340.
72. D. R. Lawver, F. D. Jackson, An accumulation of turtle eggs with embryos from the Campanian (Upper Cretaceous) Judith River Formation of Montana. *Cretac. Res.* **69**, 90–99 (2017).
73. S. Choi, N.-H. Kim, H.-I. Kim, J. J. Kweon, S. K. Lee, S. Zhang, D. J. Varricchio, Preservation of aragonite in Late Cretaceous (Campanian) turtle eggshell. *Palaeogeogr. Palaeoclimatol. Palaeoecol.* **585**, 110714 (2022).
74. Z. Zhao, Discovery of the dinosaurian eggs and footprint from Neixiang County, Henan Province. *Vert. PalAsiat.* **17**, 304–309 (1979).

Acknowledgments: We thank À. Galobart (Institut Català de Paleontologia) for leading the field trip to the Tremp Basin in 2017 and provision of access to the *Megaloolithus* eggshells; R. Wu (CUG, Wuhan) for permission to study the eggshells of *A. radiata* and *C. serpentine*, and assistance in taking the CL images; D. J. Varricchio (Montana State University) for permission to study *T. zelenitskyae*; G. Debruyn and L. D'Alba (Ghent University) for their permission to study the eggshells of *C. crocodilus*; J. Wang and J. Li (Hainan Normal University) for their permission to study the eggshell of *C. mydas*; X. Jin (IVPP) and G. Wang (PKU) for their assistance in taking the SEM images; Y. Zhu (IVPP) for assistance in preparing thin sections of the eggshells; M. Ren (IVPP) for preparing Figs. 1 and 8; M. Ohl (UU) for assistance in taking the TEM image and J. Nan (Nanjing Institute of Geology and Palaeontology, Chinese Academy of Sciences) for useful discussions. This project has received funding from the European Union's Horizon 2020 research and innovation program under grant agreement no. 101005611 for Transnational Access via the EXCITE Network conducted at UU EM and MINT facility. **Funding:** This work was supported by the National Natural Science Foundation of China (NSFC) funded by the Ministry of Science and Technology (NSFC no. 42272020 to S.Z. and S.C.), European Union's Horizon 2020 research and innovation program (grant agreement no. 101005611 for Transnational Access to S.Z.), and National Research Foundation of Korea (NRF) funded by the Ministry of Science and ICT (NRF no. 2020R1A3B2079815 to S.C. and no. RS-2024-00341420 to Y.P.). **Author contributions:** Conceptualization: S.Z., S.C., and N.-H.K. Histological study and SEM analysis: S.Z. and J.X. FIB-SEM and TEM analyses: O.P. EBSD analysis: S.C., N.-H.K., and Y.P. CL analysis: S.Z. Field work: S.Z., J.X., and A.G.S. Writing—original draft: S.Z., S.C., N.-H.K., and J.X. Writing—review and editing: S.Z., S.C., N.-H.K., J.X., Y.P., O.P., and A.G.S. Figures: S.Z., S.C., N.-H.K., and Y.P. **Competing interests:** The authors declare that they have no competing interests. **Data and materials availability:** All data needed to evaluate the conclusions in the paper are present in the paper and/or the Supplementary Materials. The dinosaur and modern avian eggshells are accessioned to IVPP and ZMNH. Raw data of the EBSD and PLM images here, including the unused ones, are available through the following DOI: 10.5061/dryad.6djh9w1cd.

Submitted 16 September 2024
Accepted 25 April 2025
Published 30 May 2025
10.1126/sciadv.adt1879